Channel estimation and transmit power control in wireless body area networks

Fabio Di Franco[1], Christos Tachtatzis[2], Robert C. Atkinson[2], Ilenia Tinnirello[1], Ian A. Glover[3]

[1]Universita Degli Studi di Palermo, Palermo 90133, Italy
[2]Strathclyde University, Glasgow G1 1XW, Scotland, UK
[3]University of Huddersfield, Huddersfield HD1 3DH, UK
E-mail: christos.tachtatzis@strath.ac.uk

Abstract: Wireless body area networks have recently received much attention because of their application to assisted living and remote patient monitoring. For these applications, energy minimisation is a critical issue since, in many cases, batteries cannot be easily replaced or recharged. Reducing energy expenditure by avoiding unnecessary high transmission power and minimising frame retransmissions is therefore crucial. In this study, a transmit power control scheme suitable for IEEE 802.15.6 networks operating in beacon mode with superframe boundaries is proposed. The transmission power is modulated, frame-by-frame, according to a run-time estimation of the channel conditions. Power measurements using the beacon frames are made periodically, providing reverse channel gain and an opportunistic fade margin, set on the basis of prior power fluctuations, is added. This approach allows tracking of the highly variable on-body to on-body propagation channel without the need to transmit additional probe frames. An experimental study based on test cases demonstrates the effectiveness of the scheme and compares its performance with alternative solutions presented in the literature.

1 Introduction

Wireless body area networks (WBANs) are an emerging application for wireless sensors. Small wireless devices are secured to the human body to monitor a wide range of physical quantities. The wireless nature of these sensors permits great flexibility in their placement. New markets are opening for these technologies in medical and health monitoring, for example, real-time measurement of heart rate and blood pressure and analysis of life signals in patients with chronic conditions.

Like many wireless sensor network (WSN) applications, the sensors are particularly energy constrained. Power-efficient implementation is therefore essential. In health monitoring, implanted devices must operate for prolonged periods of time because charging is not feasible and the selection of optimum transmission power becomes important. A device that transmits at a higher power than is strictly necessary for error free reception is wasteful of energy and leads to reduced device lifetime. Transmission at a power that is too low for adequate reception results in lost or corrupted frames and trigger retransmissions which themselves consume energy.

The channel gain experienced by most radio systems changes both with time and location. Nonetheless, many systems base their transmit power on: (i) received signal strength indication (RSSI) of a frame and (ii) whether previous frames have been received successfully or not. The success or failure of frames transmitted in the recent past provides information about the current channel state. This assumes that the channel is constant over the period of a few frames. For applications with a relatively high throughput this is a reasonable assumption.

Conventional transmit power control (TPC) algorithms are not optimised for WBAN channels. Many WBAN applications transmit frames relatively infrequently leading to increased probability of channel estimation error. Furthermore, the dynamic range of channel gain is particularly large in WBAN scenarios.

The IEEE 802.15.6 working group has recognised the challenging deployment issues of WBANs and has developed a new standard [1] targeting wireless communications in and around the human body. It defines the physical and data link layers for WBANs, but does not specify a TPC algorithm.

This paper presents a channel gain estimation algorithm and evaluates it using empirical data for the on-body to on-body propagation channel. It identifies those components affecting channel variability, and proposes, and evaluates, a TPC algorithm. The contribution of this paper is 2-fold. First, assuming that the IEEE 802.15.6 WBAN operates in beacon mode with superframe boundaries, the possibility of using the beacon power received by each sensor to predict channel gain in the subsequent scheduled access is considered. Starting from the analysis of experimental power measurements collected in a previous study [2], a predictor which adaptively filters the received beacon power according to channel variability is proposed. The filter memory is increased or reduced to adapt the memory to the propagation conditions. Secondly, a fading estimator, able to adapt to the fading conditions, is presented.

The proposed TPC scheme is evaluated for two different test cases. Using RSSI to determine transmit output power is a well-established technique. This paper differs because:

- it targets the WBAN environment;
- it employs a two-step adaptive TPC (ATPC) algorithm with superior performance, but low computation and memory requirements; and
- it is the first proposed ATPC scheme for IEEE 802.15.6 MAC.

Q1

The remainder of this paper is organised as follows. Section 2 presents related work. Section 3 presents an overview of the IEEE 802.15.6 standard. Section 4 describes the WBAN channel and introduces the channel gain predictor. Section 5 describes the fade margin estimator and evaluates the proposed ATPC for two typical BAN applications, by comparing it with a constant and a variable output power schemes presented in the literature.

2 Related work

Various studies (e.g. [3–6]) have investigated novel MAC protocols to improve energy efficiency and reliability. Interoperability is another important consideration for medical applications which proprietary MAC protocols do not fulfil. The impact of topology on reliability and energy consumption is examined in [7], in which multi-hop star networks are shown to maximise reliability at the expense of energy consumption and delay. The performance of the IEEE 802.15.6 two-hop extension is studied in [8] in terms of packet delivery ratio and reliability. The routing scheme in [9] attempts to maximise the packet delivery ratio while minimising the energy consumption and identifies the benefit of a TPC scheme that adapts to channel conditions. The RF subsystem accounts for more than 75% of total power consumed when the transmit power is -10 dBm [3]. Some investigations have focused their attention on the design of more energy efficient hardware for wireless healthcare monitoring [10] and WSNs [11]. Here we do not propose new hardware, but address an efficient interoperable ATPC algorithm.

Various TPC schemes have been described in the literature. An algorithm for WSNs is presented in [12] based on knowledge of RSSI from neighbours. Pavon and Choi [13] propose monitoring of RSSI from beacons or other frames sent by the access point and compute an average RSSI. These proposals are based on theoretical analysis or simulations assuming idealised radio models. The algorithm proposed here is based on experimental results.

Novel TPC algorithms based on the last RSSI and linear prediction of the channel are described in [14]. A comparison of different predictors (as presented in Section 4) shows that the dynamic predictor proposed in this paper outperforms linear predictors. Moreover, in this paper, the propagation characteristics, power consumption and outage for each link is analysed and presented. These are important for WBANs where shadowing of the body significantly affects channel gain. A class of adaptive power control protocols, in which the period between each feedback event is varied according to channel quality, is described in [15]. Feedback from receiver to transmitter modifies both transmitted power and the interval between feedback packets. Unfortunately, the need of continuous control packets has significant impact on energy consumption (as the authors acknowledge).

A TPC scheme for an off-body to on-body environment is presented in [16]. This scheme is based on an exponentially weighted moving-average of previous RSSI values in which the algorithm parameters are tuned for each activity to balance energy saving and reliability. The work is extended by introducing a new scenario (on-body to on-body), adding new activities and on-body positions and presenting a mechanism which automatically adjusts the tuning parameter based on channel conditions.

3 IEEE 802.15.6 networks

The IEEE 802.15.6 working group has defined a standard for short-range wireless communication designed to work on, around or in a human body. It defines narrowband (NB), ultra-wide band and human body communications (HBCs) physical layers (PHYs). Each PHY uses existing industrial scientific and medical bands as well as frequency bands approved by national medical and regulatory authorities. In particular, the NB PHY supports the new medical body area network band recently released by the Federal Communications Commission [17]. The analysis presented here is performed in this frequency band. All PHYs support a common MAC layer which can either work in beacon mode with superframe boundaries, beacon mode without superframe boundaries or non-beacon mode. Here, the focus is on beacon mode with superframe boundaries in which the hub node of a star topology is responsible of dividing the channel time into regular intervals (superframes) which are delimited by beacon transmissions.

The superframe is divided in 1–255 medium access slots with adjustable duration. The superframe starts with a beacon frame followed by two consecutive periods each consisting of an exclusive access phase, random access phase, managed access phase, an optional B2 frame and the contention access phase. The (variable) length of these phases is constraint to an integer number of allocation slots. Setting any of these lengths to zero eliminates the access phase. Here, the access phases of interest are MAP1 and MAP2 which allow devices to access the channel in a scheduled (contention-free) manner.

During scheduled access set-up, the node specifies bandwidth and power management requirements to the hub which responds with wake-up and bandwidth parameters. The scheduled allocation size and position are arbitrarily decided by the hub resulting in more flexible scheduling (higher granularity in slots, slot durations and slot positioning) than IEEE 802.15.4.

The MAC includes four frame acknowledgement policies: (i) not acknowledged (N-Ack), (ii) immediately acknowledged (I-Ack), (iii) block acknowledged later (L-Ack) and (iv) block acknowledged (B-Ack).

3.1 Scenario

A WBAN with a single hub star topology is considered. Typical node locations are shown in Fig. 1, where the hub/transmitter (TX) is placed on the chest and six nodes/receivers (RX) are located on the right abdominal side (i), right hip (ii), left side of the back (latissimus dorsi referred to as dorsi for the remainder of the paper) (iii), low centred back (iv), left arm (v) and left ankle (vi). These locations represent common on-body requirements for healthcare monitoring [18].
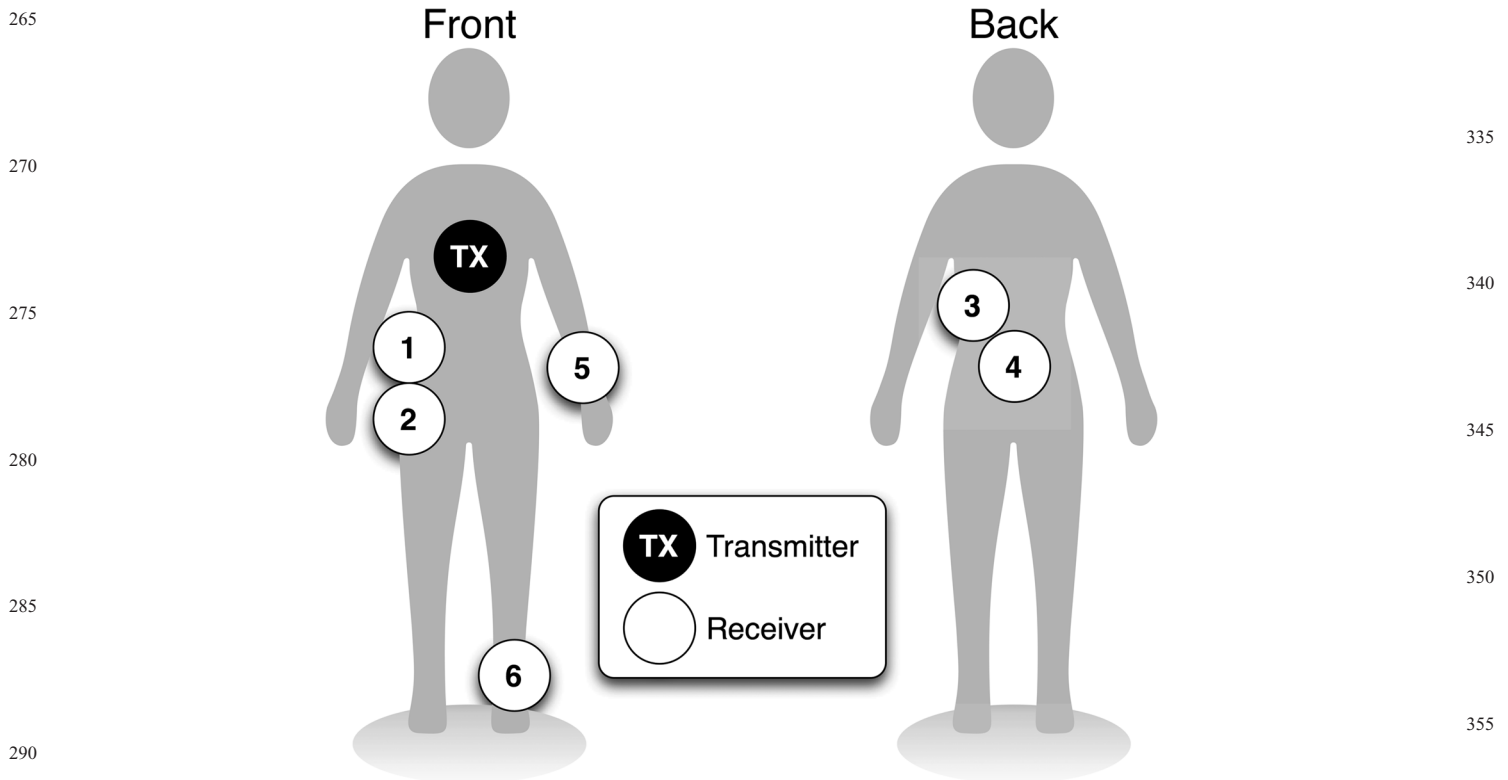
Fig. 1 *On-body positions of transmitters and receivers*

It is assumed that the sensors use an *m*-periodic scheduled access allocation scheme, where devices send a data frame every *m* superframes. During set-up the sensors send an allocation request to the hub and specify the data transfer direction (uplink), the wake-up period (*m*) and the number of allocation slots needed to complete the transfer. The hub assigns one or more allocation slots (known as an allocation interval) according to the requirements of each sensor, and sends an allocation response to indicate that the allocation interval is granted. After set-up, data are transmitted following a periodic sleep cycle as shown in Fig. 2. The sensor device is awake to receive the first beacon that indicates the start of a superframe after which it goes to sleep. Sensors sleep until $t_{W_{up}}$ seconds before the nominal start of the allocation slot to allow radio calibration. On waking, the device sends an uplink data frame, waits for a short interframe spacing (T_{SIFS}) time for an acknowledgment and then sleeps for the remainder of the current, and *m* subsequent, superframes, where devices wakes-up again to receive the *m*th beacon.

4 Channel prediction

Owing to channel variability, the channel predictor must dynamically weight the current and previous measurements to minimise prediction error. It is assumed that the hub transmits beacon frames at the maximum output power P_X (0 dBm) to ensure that all nodes in the network are able to decode the frames for synchronisation purposes. The hub is not energy constrained unlike the end devices since charging is not expected to be problematic. It is also assumed that the receiver sensitivity is known and that the channel is reciprocal [19].

4.1 Channel behaviour

The WBAN channel is subject to large variation as the body changes posture. Fig. 3 shows the temporal variation of RSSI for two links when the subject is sitting, standing, walking and running. The sensor on the ankle exhibits higher channel variability, especially when dynamic activities are performed.

The channel measurement details are described in [20]. Although these experimental results have been collected for IEEE 802.15.4 PHY, for which commercial sensors are available, it is anticipated that they will also be representative of the narrowband IEEE 802.15.6 PHY.

Channel gain is calculated by each sensor using the beacon power measured at the beginning of each superframe. As shown in Fig. 2, it is assumed that sensor transmissions are
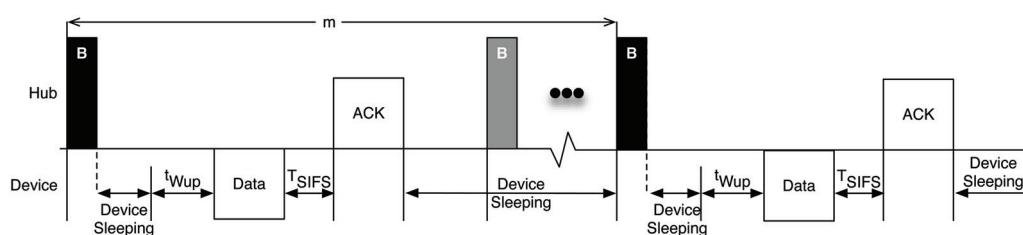

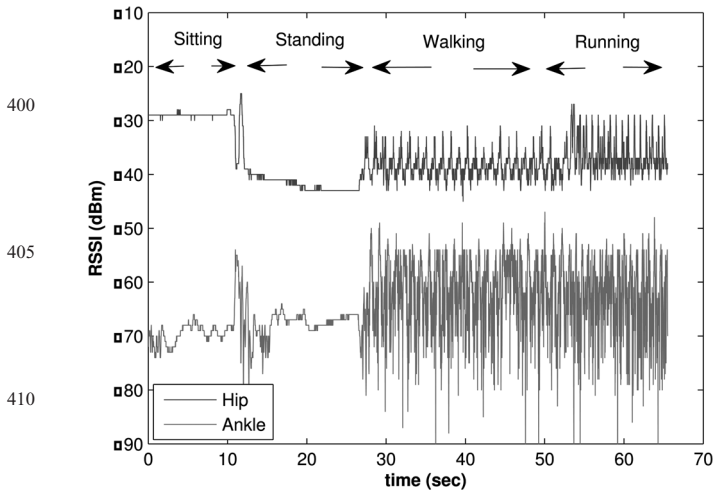**Fig. 2** *Timing diagram for m-periodic uplink allocation*

Fig. 3 *Temporal variation of the RSSI for two links when subject performs activities (chest to hip and chest to ankle)*

always followed by an immediate acknowledgement sent by the hub with maximum possible power P_X. Since the ACK transmission is separated from the data by only T_{SIFS} seconds, the channel gain is well-approximated by $RSSI_{ACK} - P_X$ where $RSSI_{ACK}$ is the ACK power measured at the receiver. This approximation is only available after the end of the allocation slot. Each sensor node regularly measures the received power of the beacons because beacon receptions are mandatory for maintaining network synchronisation. Measurement of received beacon power allows the calculation of channel gain at the beginning of each superframe using $RSSI_{Beacon} - P_X$, where $RSSI_{Beacon}$ is the beacon power measured at the receivers. Since the allocation slot granted to each sensor starts δ seconds after the beacon transmission, the estimate of channel gain is not necessarily accurate at the beginning of the slot.

It is proposed that channel gain be predicted after reception of the nth beacon frame by means of an autoregressive filter

$$\hat{C}(n, \ \delta, \ \alpha) = \alpha(n, \ \delta)\big(RSSI_{Beacon}(n) - P_X\big) \\ + (1 - \alpha(n, \ \delta))\hat{C}(n - 1, \ \delta, \ \alpha) \quad (1)$$

where $\hat{C}(n - 1, \ \delta, \ \alpha)$ is the previous channel gain estimate and α is the filter memory to be tuned according to channel variability and δ. In particular, for smaller δ or more slowly varying channels, higher values of α can be used giving more weight to the current channel sample. For larger δ or more quickly varying channels, lower values of α can be used giving more weight to the channel history.

After reception of an ACK frame, the prediction error can be evaluated by comparing the estimate with the actual channel gain

$$MSE(\delta, \ \alpha) = E\Big[\big(\hat{C}(n, \ \delta, \ \alpha) - C(n, \ \delta)\big)^2\Big] \quad (2)$$

where $C(n, \delta)$ is the actual channel gain of the data frames for superframe n with delay time-offset δ.

To test the effectiveness of the predictor channel samples reported in [20] are utilised. The sampling interval is 15 ms which allows representation of channel conditions in each allocation slot. Fig. 4 shows the prediction error observed for a superframe of 150 ms for a range of time-offsets and different sensor locations as a function of filter memory α. The error is normalised by the maximum error obtained for each location.

It can be seen that the mean square error (MSE) can be minimised by choosing an appropriate memory factor α for a given sensor location and time-offset, for example, for $\delta = 45$ ms, the MSE is minimised when α is 0.8 for the hip and 0.3 for the back. For short time-offsets, beacon RSSI is highly correlated with the channel condition in the allocation slots and higher values of α (i.e. more weight on the last measurement) yield higher accuracy. When the time-offset between beacon and data frame increases, predictions based on the last RSSI value become less reliable and historical data increase accuracy making lower α advantageous. For the hip sensor and $\alpha = 0.8$, normalised error grows from 0.13 to 0.9 as δ increases from 15 to 135 ms. The normalised MSE for small δ is smaller for the hip relative to the back location. This can be explained by the fact that the back location is not in line-of-sight with the hub and that introduces larger and faster signal variation. An optimum value of α exists which depends on sensor location and time-offset.
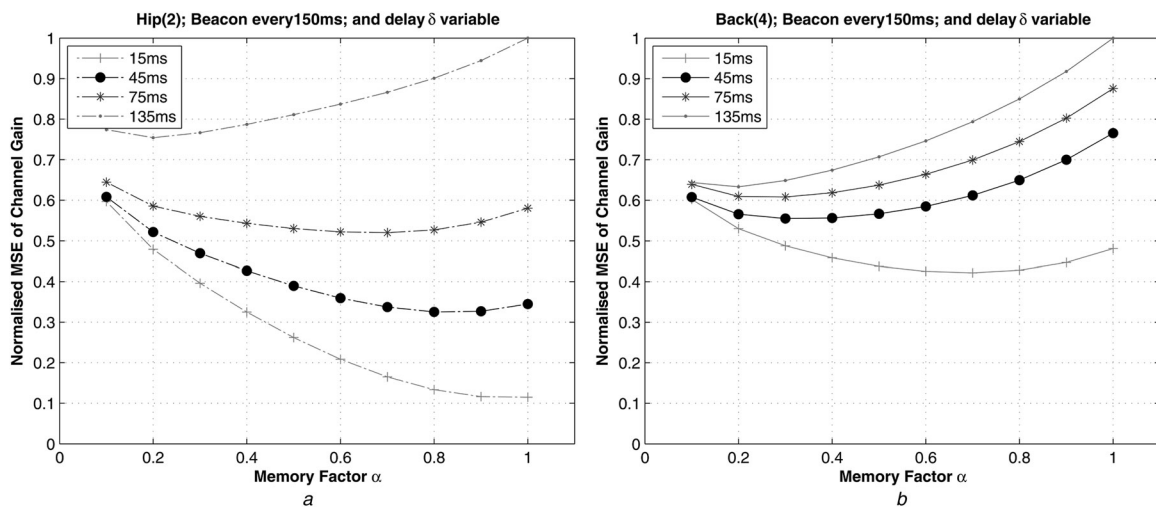

Fig. 4 *Normalised MSE against α for various body positions*

a Hip
b Back

4.2 Predictor tuning algorithm

The optimum memory factor is strongly dependent on sensor location and time-offset, and tuning is therefore necessary to minimise the estimate errors. A computationally efficient, but effective, line-search algorithm is proposed that dynamically adjusts α to minimise the MSE. In this algorithm, each node keeps track of the estimated MSE for the last N superframes. It is assumed that the hub transmits the beacon and the ACK frames at maximum power and that the channel gain does not change significantly between the data frame transmission and the acknowledgement reception (75 μs plus transmission time according to IEEE 802.15.6).

The adaptive channel gain prediction algorithm (Fig. 5 Algorithm 1) starts by assigning an initial memory factor $\alpha = 0.5$ (line 1). In every superframe, α_+ and α_- are

Q2

calculated, respectively, increasing and decreasing the current value of α by a constant ϵ (line 4). After a beacon transmission is received, three estimated channel gains are computed starting from α, α_+ and α_- (lines 5–7). Then, at the scheduled allocation interval, the frame is transmitted. After its acknowledgment is received, the MSEs are calculated (lines 9–11) and the memory factor associated to the smallest MSE becomes the new value of α at the next iteration (lines 12–21).

The best value of ϵ was determined empirically to be 0.02. To minimise the memory footprint of the algorithm, the MSEs were computed for the last five superframes.

The proposed adaptive predictor for α was compared with two constant α exponential moving-average estimators, three arithmetic moving-average estimators (with window widths of 5, 10 and 15 samples) and an estimator which only

---

Algorithm 1

1: $\alpha(0) = 0.5$.

2: **for** each superframe n **do**

3:     After beacon is received:

4:     Set $\alpha_0 = \alpha(n-1)$, $\alpha_+ = \alpha(n-1) + \epsilon$ and $\alpha_- = \alpha(n-1) - \epsilon$

    Compute channel gain predictions for α_0, α_+ and α_-:

5:     $\widehat{C}_0(n,\delta) = \alpha_0 RSSI_{Beacon}(n) + (1-\alpha_0)\widehat{C}(n-1,\delta)$

6:     $\widehat{C}_+(n,\delta) = \alpha_+ RSSI_{Beacon}(n) + (1-\alpha_+)\widehat{C}(n-1,\delta)$

7:     $\widehat{C}_-(n,\delta) = \alpha_- RSSI_{Beacon}(n) + (1-\alpha_-)\widehat{C}(n-1,\delta)$

8:     After Acknowledgement is received

    Compute MSE for α_0, α_+ and α_-:

9:     $\widehat{MSE}_0(n,\delta) = \sum_{i=0}^{N-1}[(\widehat{C}_0(n-i,\delta) - RSSI_{Ack}(n-i))^2]/N$

10:     $\widehat{MSE}_+(n,\delta) = \sum_{i=0}^{N-1}[(\widehat{C}_+(n-i,\delta) - RSSI_{Ack}(n-i))^2]/N$

11:     $\widehat{MSE}_-(n,\delta) = \sum_{i=0}^{N-1}[(\widehat{C}_-(n-i,\delta) - RSSI_{Ack}(n-i))^2]/N$

    Select the $\alpha(n)$ from the $\{\alpha_0, \alpha_+, \alpha_-\}$ based on minimum MSE

12:     **if** $\widehat{MSE}_+(n,\delta) < \widehat{MSE}_0(n,\delta)$ and $\widehat{MSE}_+(n,\delta) < \widehat{MSE}_-(n,\delta)$ **then**

13:         $\alpha(n) = \alpha+$

14:         $\widehat{C}(n,\delta) = \widehat{C}_+(n,\delta)$

15:     **else if** $\widehat{MSE}_-(n,\delta) < \widehat{MSE}_0(n,\delta)$ and $\widehat{MSE}_-(n,\delta) < \widehat{MSE}_+(n,\delta)$ **then**

16:         $\alpha(n) = \alpha-$

17:         $\widehat{C}(n,\delta) = \widehat{C}_-(n,\delta)$

18:     **else**

19:         $\alpha(n) = \alpha_0$

20:         $\widehat{C}(n,\delta) = \widehat{C}_0(n,\delta)$

21:     **end if**

22: **end for**
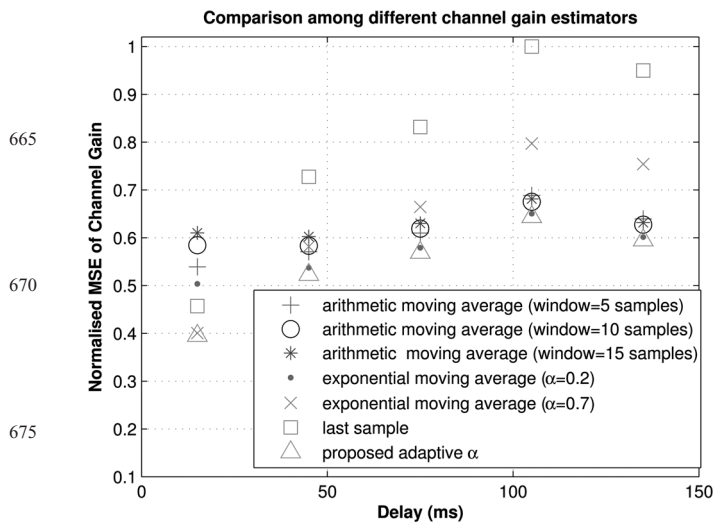

Fig. 5 *Adaptive channel gain predictor*

Fig. 6 *Comparison of channel gain predictors*

considers the RSSI of the last beacon (which can be considered an arithmetic moving-average estimator with window of 1 or an exponential moving-average estimator with $\alpha = 1$). The normalised MSE for the chest-to-back link is shown in Fig. 6. The exponential moving-average estimator with $\alpha = 0.7$ and 0.3 is optimal for that device location and for delays of 15 and 75 ms, respectively, (as shown in Fig. 4b).

The estimator which uses the RSSI of the last beacon performs well for low delays (15 ms), but poorly for higher delays. The adaptive α predictor outperforms all other estimators for all delays and the constant α exponential (see Fig. 5) moving-average estimators perform similarly in the delay regions for which their weights are optimised.

5 Transmit power control scheme

TPC algorithms add a margin to the channel gain predictions to ensure successful transmission of packets. If this margin is high, the probability of lost packets reduces at the expense of higher power consumption. A low margin increases the probability of dropped packets and hence retransmissions could outweigh any energy savings because of the lower transmission power. An optimum margin must therefore be estimated.

5.1 Fade margin estimation

The movement of the body and multipath effects mean that predicted channel gain may be significantly different from actual channel gain. The proposed adaptive channel gain predictor is able to track the bulk channel behaviour. If the transmission power is selected to be equal to the output of the estimator, the link will operate near the receiver sensitivity threshold and packet loss will occur because of the residual error of $\text{RSSI}_{\text{ACK}} - \hat{C}(n, \delta)$. The residual error was analysed to estimate a margin that will yield adequate channel reliability.

The cumulative distribution function (CDF) was considered, which measures the probability that the residual error is more than a given threshold. Fig. 7a shows the CDF of the error for all device locations and the aggregate of activities, when the time-offset δ is 15 ms and superframe duration is 150 ms. If fade margin is not added to the prediction, then the probability to underestimate the channel gain and consequently lose frames could be as high as 60%. When a fade margin of 5 dB is added (i.e. -5 dB in the graph), the predictor underestimates the channel gain with probability of 0.9 and 0.3% for the side and hip locations, respectively. For all other locations, this fade margin will reduce the probability of lost frames from 60 to $< 10\%$. In particular, the highest probability to underestimate the channel gain is for the dorsi location (9.3% at the 5 dB margin).

Fig. 7b shows the CDF of the error for the dorsi location, for each activity and delay of 15 ms that place the data frames at the beginning of the 150 ms superframe. For dynamic activities (walking and running, inside and outside a building), the probability of error for the predictor with 5 dB margin is between 10.6 and 16.3%. The static activities (sitting and standing still inside a building) experience small channel variations and no prediction errors were
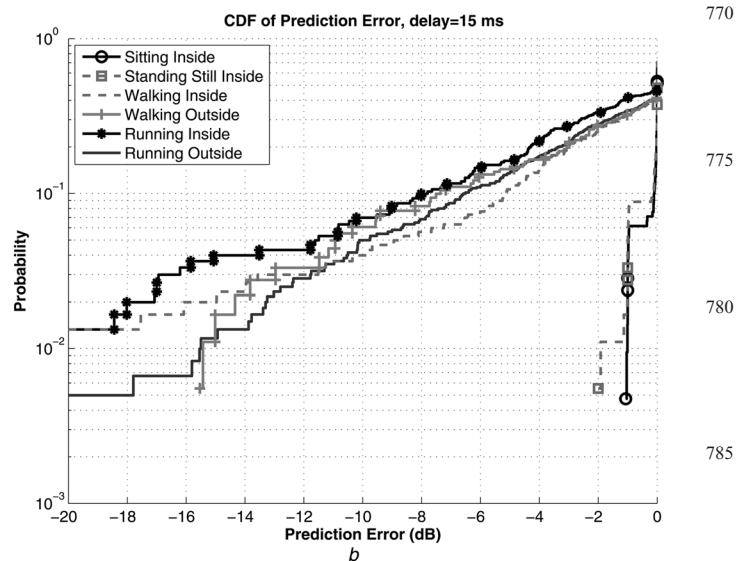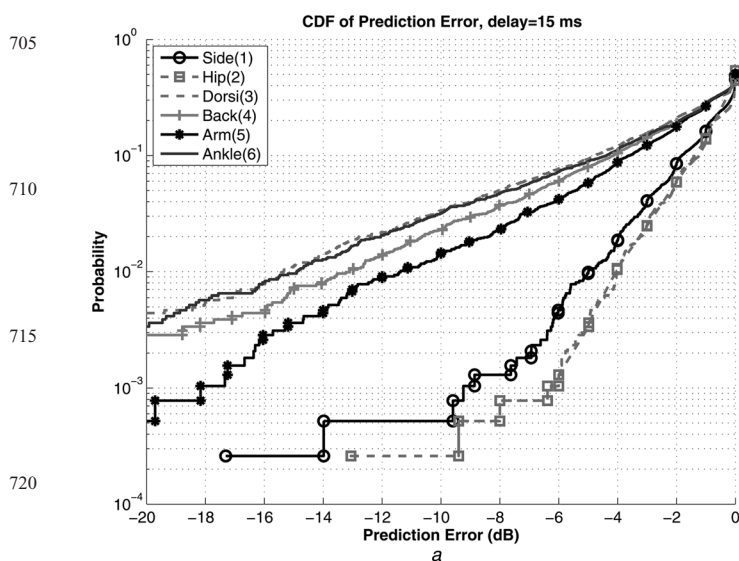

Fig. 7 *CDF of prediction error with 15 ms time-offset*
a For each body locations
b For each activity on dorsi

Algorithm 2

1: Set constants $\rho = 1dB$, $THR_L = 2dB$ and $THR_H = 4dB$

2: $\mu(0) = 3dB$

3: **for** each superframe n **do**

4:    **if** $\sqrt{\widehat{MSE}(n,\delta)} + THR_L > \mu(n-1)$ **then**

5:       $\mu(n) = \mu(n-1) + \rho$

6:    **else if** $\sqrt{\widehat{MSE}(n,\delta)} + THR_H < \mu(n-1)$ and

      $\mu(n-1) > THR_L$ **then**

7:       $\mu(n) = \mu(n-1) - \rho$

8:    **end if**

9:    **if** last data frame lost (no ACK) **then**

10:      $\mu(n) = \mu(n-1) + 3\rho$

11:   **end if**

12: **end for**

Fig. 8 *Adaptive fade margin estimator*

observed. This indicates that a margin smaller than 5 dB is adequate to ensure reliable communications. The CDF of residual error for longer time-offsets (not shown here) increases the probability of error, and consequently higher fade margin is required to ensure reliable communications.

These observations on the residual prediction error indicate that a constant fade margin is not suitable to balance the trade-off of channel reliability and energy efficiency. The adequate margin depends on the type of activity performed, the device location and the time-offset of the allocation slot. For reliable communications, static activities require small margins compared with dynamic activities. Longer time-offsets and device locations with obstructed line-of-sight require higher margins. To define an ATPC scheme that is able to determine the optimum fade margin without additional probe packets, the errors provided by the channel gain predictor can be utilised. This margin is optimised as a function of the channel gain prediction $\widehat{MSE}(n, \delta)$ (calculated in Section 4) as described in Fig. 8 Algorithm 2.

An initial fade margin $\mu(0)$ is set to 3 dB. In every superframe, the root-mean-square error $\sqrt{\widehat{MSE}(n, \delta)}$ is compared with a lower (THR_L) and an upper (THR_H) threshold. If the error is more than the last margin $\mu(n-1)$ by a threshold of THR_L, the margin is increased by ρ dB. If the error is less than the last margin by the threshold THR_H, the margin is decreased by ρ dB. The margin is decreased until the minimum threshold (THR_L) is reached. No further decreases will occur once the minimum margin is reached. When a data frame is lost in superframe $n-1$, the (see Fig. 8) margin is increased by 3ρ to ensure no further frames are lost. The values of ρ, THR_L, THR_H and THR_{min} are found experimentally.

5.2 Performance evaluation

The proposed ATPC for IEEE 802.15.6 scheduled access networks consists of two parts: the adaptive channel gain prediction (Fig. 5 Algorithm 1) and the fade margin estimation (Fig. 8 Algorithm 2).

Table 1 Power consumption in TX mode for the CC2400 transceiver ($V_{cc} = 3.0$ V)

Tx output power, dBm	0	−5	−10	−15	−20	−25
power, mW	52.0	42.0	34.0	30.0	27.5	25.5

To evaluate the performance of the ATPC scheme, a channel gain predictor and fade margin estimator were implemented and processed the experimentally collected RSSI values in [20]. A frame is lost when the sum of the channel gain and fade margin is lower than the receiver sensitivity of the CC2420 radio chip [21] which is equal to −95 dBm. The proposed algorithm alters the transmission power and experimental results have shown that reduction in the transmission power results in equal reduction to the RSSI. The device power consumption has been computed as a function of the power levels selected by the TPC scheme. The mapping between output transmit power and power consumption is summarised in Table 1. This is the effective power consumption of the CC2420 transceiver used in this experiment [21].

The proposed ATPC algorithm for a superframe of 150 ms was compared with the following:

1. Fixed TX output power equal to −10 dBm.
2. The power algorithm proposed in [16]

• conservative strategy (data loss is critical; $\alpha_d = 0.8$ and $\alpha_u = 0.2$);
• balanced strategy (data loss and energy savings have equal emphasis $\alpha_d = 0.8$ and $\alpha_u = 0.8$); and
• aggressive strategy (energy savings are critical; $\alpha_u = 0.2$ and $\alpha_u = 0.8$).

Two test cases, which are representative of typical WBAN applications, were considered:

1. An application with high reliability and strict latency requirements (<150 ms) such as ECG, EEG and EMG waveforms.
2. An application with relaxed latency requirements (<3 s) such as physiological parameters (blood pressure, heart rate, SpO_2).

In the first test case, the scheduled allocation interval is dimensioned to allow up to five immediate retransmissions in the same superframe. The link outage, calculated as the frame errors (after retransmissions) divided by the number of transmitted frames, is $<0.05\%$. The average power drawn for each transmitted frame, including the cost of retransmission, is shown in Fig. 9. It is observed that:

• For chest-side, chest-hip and chest-arm links, the ATPC algorithm saves $\sim 25\%$ of energy compared with the fixed (-10 dBm) output power. The algorithm described in [16] and the proposed algorithm show the same power consumption for these sensor locations. In these links, because of the good channel condition, the optimal transmit power is much lower than the minimum output power of the transceiver (i.e. -25 dBm in CC2420). The minimum transmit power is therefore used by both schemes.
• For chest-dorsi, chest-back and chest-ankle, ATPC saves, respectively, 20, 16 and 18% compared with the -10 dBm fixed transmit power and 4, 7 and 9% compared with the most aggressive strategy described in [16].
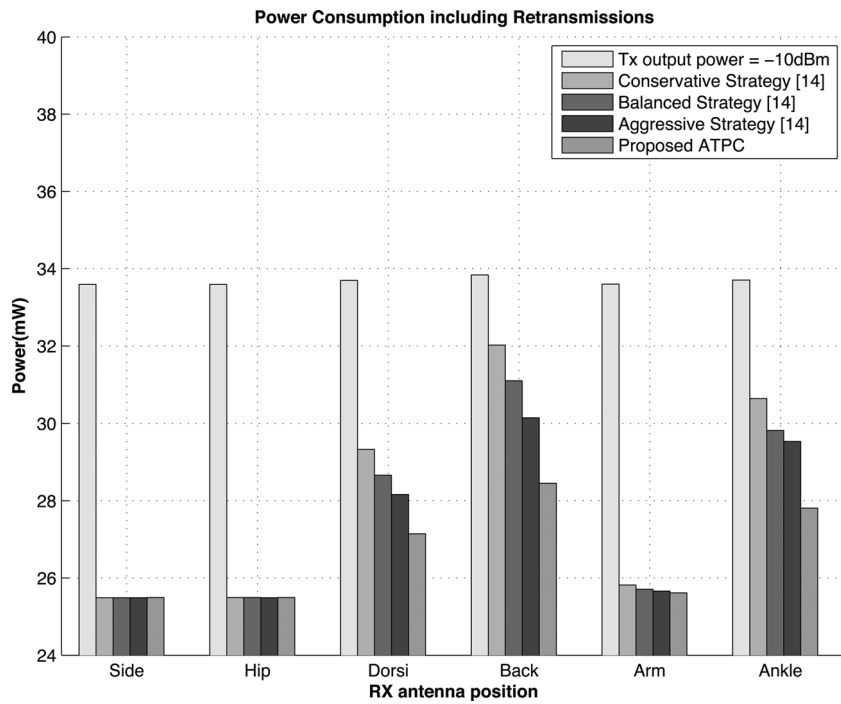
Fig. 9 *Power consumption comparison with retransmissions*

In the second test case, there are no strict latency requirements and therefore the erroneous frames will not be retransmitted at the link layer. The power consumption is calculated as the average power drawn for each frame transmitted and the link outage as the number of lost/ erroneous frames divided by the number of transmitted frames.

Figs. 10a and b show the energy consumption and frame error rate for all algorithms and body positions. These show that:

• For chest-side, chest-hip and chest-arm links, ATPC saves ∼ 25% of energy with respect to fixed output power. ATPC and the algorithm described in [16] show almost the same energy consumption because transmit output power is at the minimum power level.
• For chest-dorsi, chest-back and chest-ankle, ATPC saves, respectively, 23, 20 and 21% compared with the fixed transmit power, but at the cost of higher outage. For the chest-dorsi link, the ATPC algorithm saves 3% of energy and has similar link outage to the most aggressive strategy in [16]. For the chest-back link, ATPC saves of 7% of energy compared with the most aggressive strategy in [16], although the frame error rate increases from 4 to 5%. For the chest-ankle link, the proposed algorithm saves 3% of energy and the frame error rate decreases from 6 to 4.6% with respect to the balanced strategy in [16].
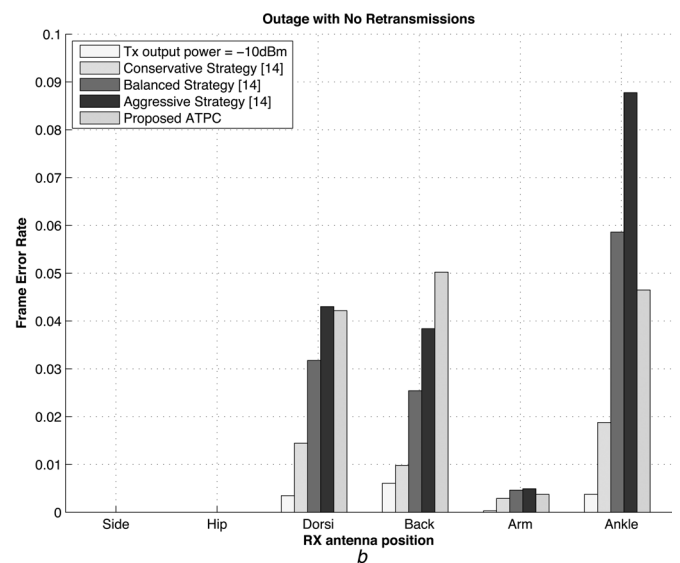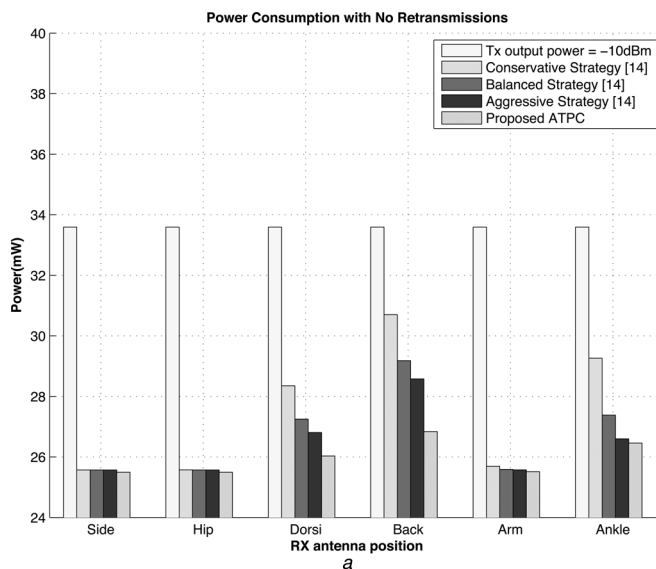

Fig. 10 *Energy consumption and frame error rate*

a Power consumption
b Link outage comparisons without retransmissions

Table 2 Proposed ATPC performance (average power consumption and link outage) for the dorsi location

No retransmission	Static activities	Dynamic activities	All activities
power consumption, mW	26.0	26.1	26.0
link outage, %	0.0	6.4	4.2
With retransmission			
power consumption, mW	26.0	28.0	27.1
link outage, %	0.0	0.0	0.0

The behaviour of the ATPC algorithm across different activities has also been compared. Table 2 shows the average power consumption and link outage for the two test cases and for the chest-dorsi link. The static activities show a virtually zero frame error rate. For dynamic activities, in the case of no retransmissions, the frame error rate is 6.4%. With retransmissions the link outage reduces to zero, but the average power consumption increases by 1.9 mW which is 7.2%. The chest-back and chest-ankle links show similar behaviour to the chest-dorsi link. Chest-side, chest-hip and chest-arm have almost zero link outage, even for dynamic activities, because of the improved channel gain.

6 Conclusion

An ATPC algorithm has been described that provides reliable, but energy efficient, operation. The proposed algorithm has been evaluated for WBANs using the IEEE 802.15.6 beacon mode with superframe boundaries. The proposed scheme does not use any probe packet and does not require any modification to the standard, making it suitable for interoperation.

The ATPC has been compared with fixed output power transmission and another WBAN TPC algorithm [16]. The comparison was performed using two typical WBAN application scenarios; an application with strict latency and high reliability and an application with relaxed latency. It has been shown that ATPC saves 16–25% of energy compared with fixed output power across different links. Against the existing WBAN power control algorithms in the literature, the energy savings were between 3 and 9% for the two applications with similar link outages, demonstrating that the proposed scheme can save energy without compromising reliability. It has been shown that link reliability for static activities is almost perfect with zero link outages and that, during dynamic activities, retransmissions can eliminate link outages at the expense of an increased power consumption of 7.2%. Delay tolerant application may not be able to afford the latency introduced by retransmissions and this must be taken in consideration when deploying the TPC algorithm. For line-of-sight links (where channel gain is good), devices can probably fix transmission power to the minimum supported by the transceiver, without significant impact on channel reliability.

Future work will be carried out to quantify the advantages of the proposed TPC algorithm for on-body to off-body links and its impact under two-hop extended star topology provision of IEEE 802.15.6.

7 References

1 IEEE 802.15.6: 'IEEE standard for local and metropolitan area networks part 15.6: wireless body area networks'. *IEEE Std 802.15.6-2012*, 2012, pp. 1–271
2 Di Franco, F., Tachtatzis, C., Graham, B., *et al.*: 'The effect of body shape and gender on wireless body area network on-body channels'. Proc. IEEE Middle East Conf. Antennas and Propagation (MECAP), Cairo, Egypt, October 2010, pp. 1–3
3 Omeni, O., Wong, A., Burdett, A., Toumazou, C.: 'Energy efficient medium access protocol for wireless medical body area sensor networks', *IEEE Trans. Biomed. Circuits Syst.*, 2008, **2**, (4), pp. 251–259
4 Li, H., Tan, J.: 'Heartbeat-driven medium-access control for body sensor networks', *IEEE Trans. Inf. Technol. Biomed.*, 2010, **14**, (1), pp. 44–51
5 Rezvani, S., Ghorashi, S.: 'Context aware and channel-based resource allocation for wireless body area networks', *IET Wirel. Sens. Syst.*, 2013, **3**, (1), pp. 16–25
6 Bouabdallah, F., Bouabdallah, N., Boutaba, R.: 'Efficient reporting node selection-based MAC protocol for wireless sensor networks', *Wirel. Netw.*, 2013, **19**, (3), pp. 373–391, URL: http://www.dx.doi.org. ejproxy.astaredu.sg/10.1007/s11276-012-0473-9
7 Natarajan, A., de, S.B., Yap, K.-K., Motani, M.: 'To hop or not to hop: network architecture for body sensor networks'. Proc. Sixth Annual IEEE Communications Society Conf. Sensor, Mesh and Ad Hoc Communications and Networks SECON 2009, New Orleans, USA, June 2009, pp. 1–9
8 Lin, C.-S., Chuang, P.-J.: 'Energy-efficient two-hop extension protocol for wireless body area networks', *IET Wirel. Sens. Syst.*, 2013, **3**, (1), pp. 37–56
9 Jacobsen, R., Kortermand, K., Zhang, Q., Toftegaard, T.: 'Understanding link behavior of non-intrusive wireless body sensor networks', *Wirel. Pers. Commun., English*, 2012, **64**, pp. 561–582, URL: http://www.dx.doi.org/10.1007/s11277-012-0601-y
10 Chen, S.-L., Lee, H.-Y., Chen, C.-A., Huang, H.-Y., Luo, C.-H.: 'Wireless body sensor network with adaptive low-power design for biometrics and healthcare applications', *IEEE Syst. J.*, 2009, **3**, (4), pp. 398–409
11 Kopta, V., Pengg, F., Le Roux, E., Enz, C.: 'A 2.4-GHz low power polar transmitter for wireless body area network applications'. Proc. IEEE 11th Int. New Circuits and Systems Conf. (NEWCAS), Paris, France, 2013, pp. 1–4
12 Jeong, J., Culler, D., Oh, J.-H.: 'Empirical analysis of transmission power control algorithms for wireless sensor networks'. Proc. Fourth Int. Conf. Networked Sensing Systems, INSS 2007, Braunschweig, Germany, June 2007, pp. 27–34
13 Pavon, J., Choi, S.: 'Link adaptation strategy for IEEE 802.11 WLAN via received signal strength measurement'. Proc. IEEE Int. Conf. Communications, ICC 2003, Anchorage, Alaska, USA, May 2003, vol. 2, pp. 1108–1113
14 Smith, D., Hanlen, L., Miniutti, D.: 'Transmit power control for wireless body area networks using novel channel prediction'. Proc. IEEE Wireless Communications and Networking Conf. (WCNC), Paris, France, April 2012, pp. 684–688
15 Moulton, B., Hanlen, L., Chen, J., Croucher, G., Mahendran, L., Varis, A.: 'Body-area-network transmission power control using variable adaptive feedback periodicity'. Proc. Communications Theory Workshop (AusCTW), Australian, February 2010, pp. 139–144
16 Xiao, S., Dhamdhere, A., Sivaraman, V., Burdett, A.: 'Transmission power control in body area sensor networks for healthcare monitoring', *IEEE J. Sel. Areas Commun.*, 2009, **27**, (1), pp. 37–48
17 FCC 12-54: Amendment of the Commission's Rules to Provide Spectrum for the Operation of Medical Body Area Networks
18 Latr, B., Braem, B., Moerman, I., Blondia, C., Demeester, P.: 'A survey on wireless body area networks', *Wirel. Netw. English*, 2011, **17**, pp. 1–18, URL: http://www.dx.doi.org/10.1007/s11276-010-0252-4
19 Hanlen, L., Chaganti, V., Gilbert, B., Rodda, D., Lamahewa, T., Smith, D.: 'Open-source testbed for body area networks: 200 sample/sec, 12 hrs continuous measurement'. Proc. IEEE 21st Int. Symp. Personal, Indoor and Mobile Radio Communications Workshops (PIMRC Workshops), Istanbul, Turkey, September 2010, pp. 66–71
20 Di Franco, F., Tachtatzis, C., Graham, B., Tracey, D., Timmons, N., Morrison, J.: 'On-body to on-body channel characterization'. Proc. IEEE Sensors, Limerick, Ireland, October 2011, pp. 908–911
21 *CC2420 Single-Chip 2.4 GHz IEEE 802.15.4 Compliant and ZigBee Ready RF Transceiver*, URL: http://www. ti.com/product/cc2420

WSS20130070

Author Queries

Fabio Di Franco, Christos Tachtatzis, Robert C. Atkinson, Ilenia Tinnirello, Ian A. Glover

Q1   Please define the acronyms MAC, ECG, EEG and EMG.

Q2   Algorithm 1 has been changed to Fig. 5 and figures are renumbered subsequently.